Frequency Analysis of Cascade-Connected Planar Transmission Lines by *ETS* Method

Biljana P. Sto{ić and Miodrag V. Gmitrović

Abstract – **The Equivalent Thevenin Source (*ETS*) method is used for frequency analysis of a two-dimensional circuit designed as cascade-connected uniform transmission lines with various widths and lengths. The efficiency and accuracy of the procedure suggested here is shown on a few various microstrip examples, such as open-ended line, line terminated in its characteristic impedance, *T*-junction and lowpass filters.**

Keywords – **Planar transmission lines, Cascade connection, *ETS* method**

I. INTRODUCTION

Electrical circuits containing microwave lines can be modeled by one-dimensional (*1D*) circuits composed of transmission lines. The analysis of such circuits in the frequency domain is simple and very fast. Sometimes, the results of analysis differ very much from the desired accurate results. This happens due to the appearance of discontinuities that are the result of different physical dimensions and shapes of the line. Because of that, more accurate, but also more complex methods, based on two-dimensional (*2D*) and three-dimensional (*3D*) approaches to the analysis of circuits containing microwave lines, are used. For that purpose, a number of approaches are developed, and some of them are given in the papers [1-9]. Also, a number of software packages are developed, such as Libra [10], *ADS* [11], *GENESYS* [12], *FAMIL* [2], etc.

A *2D* circuit can represent an equivalent electrical model of both planar microwave structures and microelectronic connections. Modeling of planar microwave structures based on an equivalent circuit consisting of elements with lumped *RLGC* parameters is used very frequently because of the simplicity of the model. But, the equivalent circuit can be very complex with many nodes and the solving of such a circuit is a very complex task. An analysis of such circuits by standard procedures requires large memory resources and takes a long time. In this paper, another efficient method of frequency analysis based on decomposition of the whole *2D* circuit in less complex multi-port ladder subnetworks and equivalent Thevenin sources for solving multi-port subnetworks, is described.

The suggested frequency analysis procedure of planar transmission lines can be used for the analysis of various microstrip structures. Various types of discontinuities occur in the conductor of planar transmission lines, such as microstrips. Some examples of microstrip structures in which these discontinuities occur frequently, are shown in Fig.1 [13].

The authors are with the Faculty of Electronic Engineering, University of Ni{, Aleksandra Medvedeva 14, 18000 Ni{, Serbia and Montenegro.

E-mails: bilja@elfak.ni.ac.yu and gmitrovic@elfak.ni.ac.yu

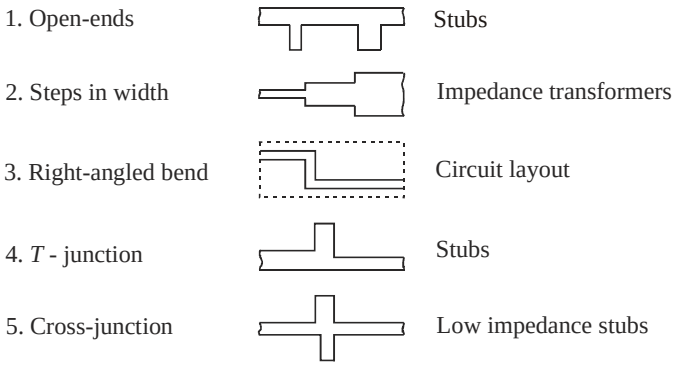

Fig.1. Various types of microstrip discontinuities and their typical circuit applications.

II. PLANAR TRANSMISSION LINE SEGMENTATION

A transmission line with given geometrical and substrate parameters can be modeled in a few ways starting with calculated characteristic impedance Z_c and effective dielectric constant ε_r^{eff}. A modeling method used here is the segmentation of the line in longitudinal and transversal directions. That way, a *2L*-port equivalent electrical network of the transmission line can be formed [1,2].

A rectangular microstrip line of a width of w and a length of d can be divided into $L \times K$ segments, as shown in Fig.2. The model of the equivalent network of a four-port segment is shown in Fig.3, and the model of a three-port segment is shown in Fig.4.

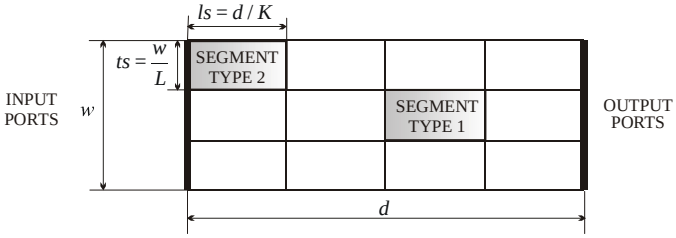

Fig.2. Segmentation of a microstrip line in transversal and longitudinal directions.

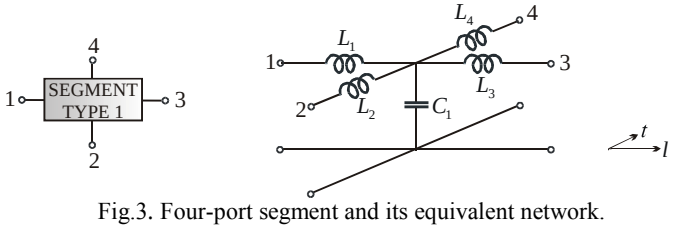

Fig.3. Four-port segment and its equivalent network.

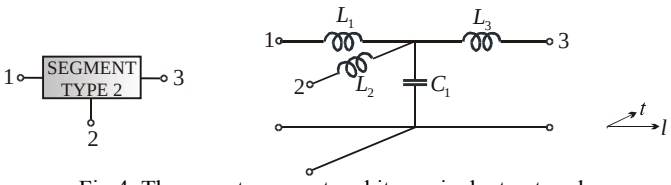

Fig.4. Three-port segment and its equivalent network.

The general solutions to frequency independent serial inductances and shunt capacitance of Figs. 3 and 4, for a microstrip line with $2L$ ports, are [1]

$$C_1 = \frac{d\sqrt{\varepsilon_r^{eff}}}{c_0 Z_c} \cdot \frac{1}{K \cdot L}, \tag{1}$$

$$L_1 = L_3 = \frac{Z_c d\sqrt{\varepsilon_r^{eff}}}{2c_0} \cdot \frac{L}{K}, \quad L_2 = L_4 = \frac{Z_c w^2 \sqrt{\varepsilon_r^{eff}}}{2c_0 d} \cdot \frac{K}{L}, \tag{2}$$

where c_0 is the velocity of propagation on the line in free medium.

A two-dimensional equivalent electrical circuit of transmission line can be obtained by properly connected equivalent networks for all three- and four-port segments.

III. Two-Dimensional *RLGC* Circuit and its Decomposition into Ladder Subnetworks

A lossless planar transmission line modeled by a *2D* circuit with *LC* lumped elements is shown in Fig.5. The circuit can be excited by several real voltage sources and terminated by several real loads. The circuit can be observed as $K+3$ cascade-connected ladder subnetworks with *2L* ports. The first subnetwork corresponds to the sources, subnetworks from 2 to $K+2$ correspond to the transmission line, and the $K+3^{rd}$ subnetwork corresponds to the loads.

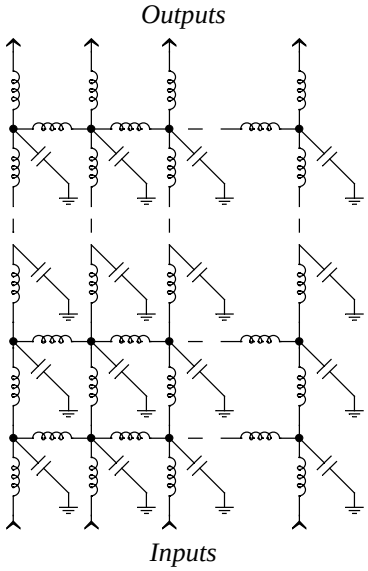

Fig.5. *2D* electrical circuit.

One ladder subnetwork, obtained from the circuit given in Fig.5, can be treated as a multi-port subnetwork with *L* input and *L* output ports as shown in Fig.6.

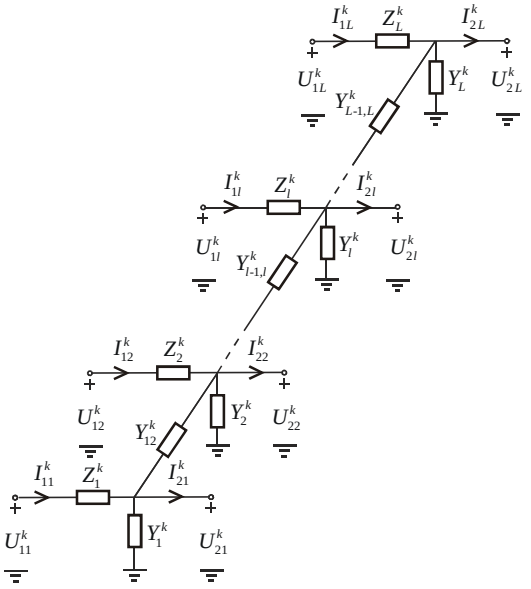

Fig.6. k^{th} ladder subnetwork with $2L$ ports.

In Fig.6, a k^{th} ladder subnetwork for planar transmission line with losses is depicted. The immittances Z_l^k, $l=1,2,\cdots,L$, $Y_{l,l+1}^k$, $l=1,2,\cdots,L-1$, correspond to the serial connections of resistors, inductors and capacitors, and the admittances Y_l^k, $l=1,2,\cdots,L$, $k=1,2,\cdots,K+3$ correspond to the shunt connections of conductances, capacitors and inductors [2,3].

IV. Transmission Matrices of Ladder Subnetworks

A terminal behaviour of the ladder subnetwork, shown in Fig.6, can be described completely by the transmission matrices. This is conveniently achieved trough the chain matrix that relates the input voltages and currents of the subnetwork to its output voltages and currents. The matrix equations are [3]

$$\boldsymbol{U}_1^k = \boldsymbol{A}_k \cdot \boldsymbol{U}_2^k + \boldsymbol{B}_k \cdot \boldsymbol{I}_2^k, \tag{3}$$

$$\boldsymbol{I}_1^k = \boldsymbol{C}_k \cdot \boldsymbol{U}_2^k + \boldsymbol{D}_k \cdot \boldsymbol{I}_2^k, \tag{4}$$

where $\boldsymbol{A}_k$, $\boldsymbol{B}_k$, $\boldsymbol{C}_k$ and $\boldsymbol{D}_k$ are transmission matrices of the ladder subnetwork. The input voltage and current vectors are $\boldsymbol{U}_1^k = \left[U_{11}^k \;\; U_{12}^k \cdots U_{1L}^k\right]^T$ and $\boldsymbol{I}_1^k = \left[I_{11}^k \;\; I_{12}^k \cdots I_{1L}^k\right]^T$, respectively.

The matrix $\boldsymbol{B}_k$ is a diagonal matrix, $B_{i,i}^k = Z_i^k$, $i=1,2,\cdots,L$. The elements of the matrices $\boldsymbol{C}_k$ and $\boldsymbol{A}_k$, which differ from zero, for $Y_{0,1}^k = Y_{L,L+1}^k = 0$, are $C_{i,i}^k = Y_i^k + Y_{i-1,i}^k + Y_{i,i+1}^k$, $A_{i,i}^k = 1 + Z_i^k \cdot C_{i,i}^k$, $i=1,2,\cdots,L$, $C_{i,i+1}^k = C_{i+1,i}^k = -Y_{i,i+1}^k$, $A_{i,i+1}^k = Z_i^k \cdot C_{i,i+1}^k$, $A_{i+1,i}^k = Z_{i+1}^k \cdot C_{i,i+1}^k$, $i=1,2,\cdots,L-1$. The transmission matrix $\boldsymbol{D}_k = \boldsymbol{1}$ is an identity matrix and $k=1,2,\cdots,K+3$.

V. *ETS* VOLTAGE AND IMPEDANCE CALCULATION OF TRANSMISSION LINES

The frequency analysis of a *2D* transmission line equivalent circuit using transmission matrices can be done by the Equivalent Thevenin Source (*ETS*) method. The analysis is based on decomposition of that circuit in cascade-connected ladder subnetworks with $2L$ ports. For each ladder subnetwork, corresponding transmission matrices are calculated and all previously subnetworks are then substituted by L *ETS*. They represent the excitation of the next ladder subnetwork. The input and output voltages, as well as the input currents of each subnetwork, can be obtained by successive application of this approach.

The voltages and output impedances of the *ETS* for the k^{th} ladder subnetwork are calculated by using recurrent relations [3]

$$\boldsymbol{U}_{2T}^{k} = [\boldsymbol{A}_k + \boldsymbol{Z}_{2T}^{k-1} \cdot \boldsymbol{C}_k]^{-1} \cdot \boldsymbol{U}_{2T}^{k-1}, \tag{5}$$

$$\boldsymbol{Z}_{2T}^{k} = [\boldsymbol{A}_k + \boldsymbol{Z}_{2T}^{k-1} \cdot \boldsymbol{C}_k]^{-1} \cdot [\boldsymbol{B}_k + \boldsymbol{Z}_{2T}^{k-1} \cdot \boldsymbol{D}_k], \tag{6}$$

where $k = 1,2,\cdots,K+3$.

The input admittance matrix is

$$\boldsymbol{Y}_1^{k} = \left[\boldsymbol{C}_k + \boldsymbol{D}_k \cdot \boldsymbol{Y}_1^{k+1}\right] \cdot \left[\boldsymbol{A}_k + \boldsymbol{B}_k \cdot \boldsymbol{Y}_1^{k+1}\right]^{-1}, \tag{7}$$

where $\boldsymbol{Y}_1^{K+3} = \boldsymbol{G}_L$ represents the diagonal matrix of loads and $k = K+2, K+1, \cdots, 2$. The voltage and current vectors at the input ports of the k^{th} ladder subnetwork are obtained simply from relations

$$\boldsymbol{U}_1^{k} = \left[\boldsymbol{1} + \boldsymbol{Z}_{2T}^{k-1} \cdot \boldsymbol{Y}_1^{k}\right]^{-1} \cdot \boldsymbol{U}_{2T}^{k-1}, \tag{8}$$

$$\boldsymbol{I}_1^{k} = \boldsymbol{Y}_1^{k} \cdot \boldsymbol{U}_1^{k}, \tag{9}$$

where $k = 1,2,\cdots,K+3$.

VI. MULTI-PORT NETWORK DRIVEN BY CURRENT AND VOLTAGE SOURCES

Consider a multi-port ladder subnetwork shown in Fig.7, [4], driven by $m1+m2$ voltage and k current real sources. In that case, the number of input ports is $L = m1+k+m2$.

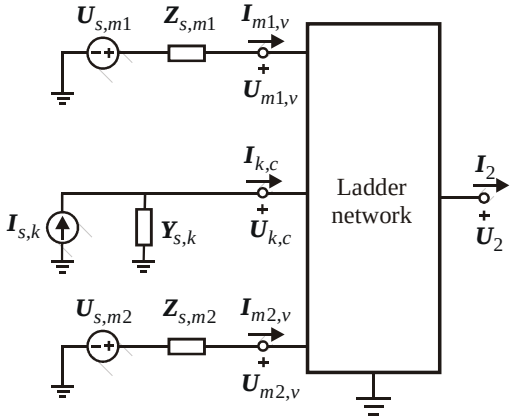

Fig.7. Multi-port ladder network driven by voltage and current real sources.

The input voltage vector of the network according to source disposition is

$$\boldsymbol{U}_1 = \underset{1\cdots m1}{[\ \boldsymbol{U}_{m1,v}} \mid \underset{1\ \cdots\ k}{\boldsymbol{U}_{k,c}} \mid \underset{1\cdots m2}{\boldsymbol{U}_{m2,v}}]^T = [U_{11}\ U_{12}\cdots U_{1L}]. \tag{10}$$

The first sign of subscripts in the vector indicates the number of the sources and the second the type of source (v - voltage and c - current source).

Also, the output voltage vector of the network can be divided as follows:

$$\boldsymbol{U}_2 = [\boldsymbol{U}_{2,m1} \mid \boldsymbol{U}_{2,k} \mid \boldsymbol{U}_{2,m2}]^T = [U_{21}\ U_{22}\cdots U_{2L}]^T. \tag{11}$$

In order to find the voltage vector $\boldsymbol{U}_{2T}$ for an open-ended network and the impedance matrix $\boldsymbol{Z}_{2T}$ for annulled sources by the *ETS* method, it is necessary to form the real input vector with known voltage vectors, $\boldsymbol{U}_{m1,v}$ and $\boldsymbol{U}_{m2,v}$ and current vector, $\boldsymbol{I}_{k,c}$. Because of that, permutation of corresponding rows in the existing transmission matrices must be done. After the row permutation is done, the equation system (3–4) becomes

$$\begin{bmatrix} \boldsymbol{U}_{m1,v} \\ \boldsymbol{I}_{k,c} \\ \boldsymbol{U}_{m2,v} \end{bmatrix} = \begin{bmatrix} \boldsymbol{U}_{s,m1} - \boldsymbol{Z}_{s,m1} \cdot \boldsymbol{I}_{m1,v} \\ \boldsymbol{I}_{s,k} - \boldsymbol{Y}_{s,k} \cdot \boldsymbol{U}_{k,c} \\ \boldsymbol{U}_{s,m2} - \boldsymbol{Z}_{s,m2} \cdot \boldsymbol{I}_{m2,v} \end{bmatrix} =$$

$$= \begin{bmatrix} \boldsymbol{A}_{m1,m1} & \boldsymbol{A}_{m1,k} & \boldsymbol{A}_{m1,m2} \\ \boldsymbol{C}_{k,m1} & \boldsymbol{C}_{k,k} & \boldsymbol{C}_{k,m2} \\ \boldsymbol{A}_{m2,m1} & \boldsymbol{A}_{m2,k} & \boldsymbol{A}_{m2,m2} \end{bmatrix} \cdot \begin{bmatrix} \boldsymbol{U}_{2,m1} \\ \boldsymbol{U}_{2,k} \\ \boldsymbol{U}_{2,m2} \end{bmatrix} + \tag{12}$$

$$+ \begin{bmatrix} \boldsymbol{B}_{m1,m1} & \boldsymbol{B}_{m1,k} & \boldsymbol{B}_{m1,m2} \\ \boldsymbol{D}_{k,m1} & \boldsymbol{D}_{k,k} & \boldsymbol{D}_{k,m2} \\ \boldsymbol{B}_{m2,m1} & \boldsymbol{B}_{m2,k} & \boldsymbol{B}_{m2,m2} \end{bmatrix} \cdot \begin{bmatrix} \boldsymbol{I}_{2,m1} \\ \boldsymbol{I}_{2,k} \\ \boldsymbol{I}_{2,m2} \end{bmatrix}$$

$$\begin{bmatrix} \boldsymbol{I}_{m1,v} \\ \boldsymbol{U}_{k,c} \\ \boldsymbol{I}_{m2,v} \end{bmatrix} = \begin{bmatrix} \boldsymbol{C}_{m1,m1} & \boldsymbol{C}_{m1,k} & \boldsymbol{C}_{m1,m2} \\ \boldsymbol{A}_{k,m1} & \boldsymbol{A}_{k,k} & \boldsymbol{A}_{k,m2} \\ \boldsymbol{C}_{m2,m1} & \boldsymbol{C}_{m2,k} & \boldsymbol{C}_{m2,m2} \end{bmatrix} \cdot \begin{bmatrix} \boldsymbol{U}_{2,m1} \\ \boldsymbol{U}_{2,k} \\ \boldsymbol{U}_{2,m2} \end{bmatrix} +$$

$$+ \begin{bmatrix} \boldsymbol{D}_{m1,m1} & \boldsymbol{D}_{m1,k} & \boldsymbol{D}_{m1,m2} \\ \boldsymbol{B}_{k,m1} & \boldsymbol{B}_{k,k} & \boldsymbol{B}_{k,m2} \\ \boldsymbol{D}_{m2,m1} & \boldsymbol{D}_{m2,k} & \boldsymbol{D}_{m2,m2} \end{bmatrix} \cdot \begin{bmatrix} \boldsymbol{I}_{2,m1} \\ \boldsymbol{I}_{2,k} \\ \boldsymbol{I}_{2,m2} \end{bmatrix} \tag{13}$$

There are no changes in the output voltage and current vectors after the row permutations. The only changes are in the corresponding transmission matrices.

After taking the new signs for transmission matrices with permuted rows $\boldsymbol{A}^{\boldsymbol{i}}$, $\boldsymbol{B}^{\boldsymbol{i}}$, $\boldsymbol{C}^{\boldsymbol{i}}$ and $\boldsymbol{D}^{\boldsymbol{i}}$ and for matrices

$$\boldsymbol{W}_s = \begin{bmatrix} \boldsymbol{Z}_{s,m1} & \boldsymbol{0} & \boldsymbol{0} \\ \boldsymbol{0} & \boldsymbol{Y}_{s,k} & \boldsymbol{0} \\ \boldsymbol{0} & \boldsymbol{0} & \boldsymbol{Z}_{s,m2} \end{bmatrix},\ \boldsymbol{S} = \begin{bmatrix} \boldsymbol{U}_{s,m1} \\ \boldsymbol{I}_{s,k} \\ \boldsymbol{U}_{s,m2} \end{bmatrix},\ \boldsymbol{S}_{v,c} = \begin{bmatrix} \boldsymbol{I}_{m1,v} \\ \boldsymbol{U}_{k,c} \\ \boldsymbol{I}_{m2,v} \end{bmatrix} \tag{14}$$

the equation system (12-13) can be written as

$$\boldsymbol{S} - \boldsymbol{W}_s \cdot \boldsymbol{S}_{v,c} = \boldsymbol{A}^{\boldsymbol{i}} \cdot \boldsymbol{U}_2 + \boldsymbol{B}^{\boldsymbol{i}} \cdot \boldsymbol{I}_2, \tag{15}$$

$$\boldsymbol{S}_{v,c} = \boldsymbol{C}^{\boldsymbol{i}} \cdot \boldsymbol{U}_2 + \boldsymbol{D}^{\boldsymbol{i}} \cdot \boldsymbol{I}_2. \tag{16}$$

The *ETS* voltage vector for an open-ended network is

$$\boldsymbol{U}_{2T} = \left[\boldsymbol{A^i} + \boldsymbol{W}_s \cdot \boldsymbol{C^i}\right]^{-1} \cdot \boldsymbol{S} \quad (17)$$

and the *ETS* impedance matrix for annulled current and voltage sources is

$$\boldsymbol{Z}_{2T} = \left[\boldsymbol{A^i} + \boldsymbol{W}_s \cdot \boldsymbol{C^i}\right]^{-1} \cdot \left[\boldsymbol{B^i} + \boldsymbol{W}_s \cdot \boldsymbol{D^i}\right]. \quad (18)$$

The relations (17) and (18) are equivalent to the recurrent relations (5) and (6), where $\boldsymbol{U}_{2T}^{k-1} \equiv \boldsymbol{S}$ and $\boldsymbol{Z}_{2T}^{k-1} \equiv \boldsymbol{W}_s$.

VII. *ETS* FOR INCREASED WIDTH LINES

The microstrip structure that comprises a junction with an increased number of input ports of corresponding networks is shown in Fig.8, where $L_1 > L$ [4]. The network is driven by $k1 + k2$ current and L voltage real sources and has $2L_1$ ports, $L_1 = k1 + L + k2$. The first k cascade-connected subnetworks with the same number of input and output ports are substituted by their L *ETS* and the last subnetwork designated by $\boldsymbol{Z}_L$ corresponds to loads.

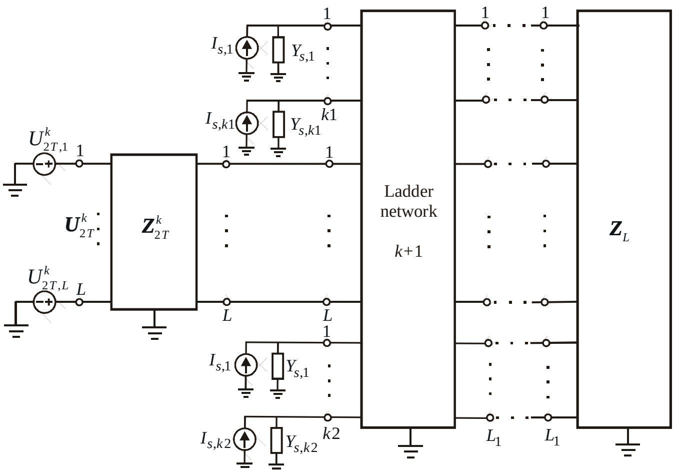

Fig.8. Microstrip structure with a junction of two networks with an increased number of ports.

The source vector of the next $k+1^{st}$ network is the voltage vector obtained by (5) increased in the form

$$\boldsymbol{U}_s = \left[0 \cdots 0 \,|\, U_{2T,1}^k \cdots U_{2T,L}^k \,|\, 0 \cdots 0\right]^T = \left[\boldsymbol{0} \,|\, \boldsymbol{U}_{2T}^k \,|\, \boldsymbol{0}\right]^T, \quad (19)$$

$$\scriptstyle 1 \cdots k1 \,|\, 1 \quad \cdots \quad L \,|\, 1 \cdots k2$$

where $\boldsymbol{0}$ is the zero vector.

According to the network connection given in Fig.8, the source impedance matrix for the next $k+1^{st}$ network is the impedance matrix obtained by (6) increased in the form

$$\boldsymbol{Z}_s = \begin{bmatrix} \boldsymbol{0} & | & \boldsymbol{0} & | & \boldsymbol{0} \\ -- & | & --- & | & -- \\ \boldsymbol{0} & | & \boldsymbol{Z}_{2T}^k & | & \boldsymbol{0} \\ -- & | & --- & | & -- \\ \boldsymbol{0} & | & \boldsymbol{0} & | & \boldsymbol{0} \end{bmatrix} \begin{matrix} 1 \\ \vdots \\ k1 \\ --- \\ 1 \\ \vdots \\ L \\ --- \\ 1 \\ \vdots \\ k2 \end{matrix}, \quad (20)$$

$$\scriptstyle 1 \cdots k1 \,|\, 1 \quad \cdots \quad L \,|\, 1 \cdots k2$$

where $\boldsymbol{0}$ is the zero matrix.

The *ETS* voltage vector and impedance matrix for the $k+1^{st}$ open-ended network are

$$\boldsymbol{U}_{2T}^{k+1} = [\boldsymbol{A}_{k+1}^i + \boldsymbol{Z}_s \cdot \boldsymbol{C}_{k+1}^i]^{-1} \cdot \boldsymbol{U}_s \quad (21)$$

and

$$\boldsymbol{Z}_{2T}^{k+1} = [\boldsymbol{A}_{k+1}^i + \boldsymbol{Z}_s \cdot \boldsymbol{C}_{k+1}^i]^{-1} \cdot [\boldsymbol{B}_{k+1}^i + \boldsymbol{Z}_s \cdot \boldsymbol{D}_{k+1}^i]. \quad (22)$$

The procedure for the solution of cascade-connected networks with an increased number of ports is as follows:

1. The relations (5) and (6) are used to obtain $\boldsymbol{U}_{2T}^k$ and $\boldsymbol{Z}_{2T}^k$, i.e. *ETS* voltages and impedances for the first k cascade-connected networks with the same number of input and output ports. This vector and matrix are used for the input ports of the next $k+1^{st}$ cascade-connected network.
2. Because of the current and voltage sources, i.e. the network junction, permutation of rows in the transmission matrices for $k+1^{st}$ network **only** must be done. The new matrices $\boldsymbol{A}_{k+1}^i$, $\boldsymbol{B}_{k+1}^i$, $\boldsymbol{C}_{k+1}^i$ and $\boldsymbol{D}_{k+1}^i$ with permuted corresponding rows are formed for the $k+1^{st}$ network with $2L_1$ ports, as shown in section VI.
3. At the junction between k^{th} and $k+1^{st}$ networks, because of the increased number of input ports, it is necessary to increase the vector $\boldsymbol{U}_{2T}^k$ and the matrix $\boldsymbol{Z}_{2T}^k$ as shown in relations (19) and (20). The voltage vector $\boldsymbol{U}_{2T}^{k+1}$ and impedance matrix $\boldsymbol{Z}_{2T}^{k+1}$ are calculated from relations (21) and (22).
4. For further calculations, $k+2, k+3, ..., K+3$, the relations (5) and (6) can be used for solving the rest of the networks in the cascade connection. All transmission matrices to the end are square matrices of sizes $L_1 \times L_1$ and forms given in the equations (3) and (4).

VIII. *ETS* FOR REDUCED WIDTH LINES

The microstrip structure with a junction of two networks with reduced number of input ports is shown in Fig.9, where $L_1 < L$, $L_1 = n - m + 1$ [5]. The first k cascade-connected subnetworks with the same number of input and output ports are substituted by L *ETS* and the last subnetwork designated by $\boldsymbol{Z}_L$ corresponds to loads.

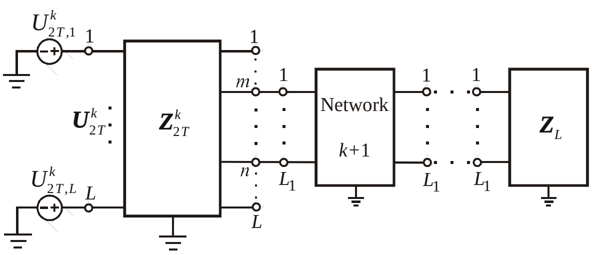

Fig.9. Cascade connection of networks with a reduced

number of ports.

The impedance matrix obtained by the equation (6) is a full matrix, and according to the network connection given in Fig.9, it can be divided in the following form:

$$\boldsymbol{Z}_{2T}^{k}=\begin{bmatrix} Z_{11}^{k} & \cdots & Z_{1L}^{k} \\ \vdots & \ddots & \vdots \\ Z_{L1}^{k} & \cdots & Z_{LL}^{k} \end{bmatrix}=\begin{array}{c}\left[\begin{array}{c|c|c} \boldsymbol{Z}_{11}^{k} & \boldsymbol{Z}_{12}^{k} & \boldsymbol{Z}_{13}^{k} \\ - & -- & - \\ \boldsymbol{Z}_{21}^{k} & \boldsymbol{Z}_{22}^{k} & \boldsymbol{Z}_{23}^{k} \\ - & -- & - \\ \boldsymbol{Z}_{31}^{k} & \boldsymbol{Z}_{32}^{k} & \boldsymbol{Z}_{33}^{k} \end{array}\right]\begin{array}{c}1\\ \vdots \\ m-1 \\ \hline m \\ \vdots \\ n \\ \hline n+1 \\ \vdots \\ L\end{array} \\ 1\cdots m-1 \,|\, m \;\cdots\; n \,|\, n+1\cdots L\end{array} \quad (23)$$

The *ETS* voltage vector at k^{th} open-ended network is a full vector and can be divided as follows:

$$\begin{aligned}\boldsymbol{U}_{2T}^{k}&=\left[U_{2T,1}^{k}\cdots U_{2T,m-1}^{k}\,|\,U_{2T,m}^{k}\cdots U_{2T,n}^{k}\,|\,U_{2T,n+1}^{k}\cdots U_{2T,L}^{k}\right]^{T}\\&=\left[\boldsymbol{U}_{2T,1}^{k}\,|\,\boldsymbol{U}_{2T,2}^{k}\,|\,\boldsymbol{U}_{2T,3}^{k}\right]^{T}\end{aligned} \quad (24)$$

The transmission matrices of the $k+1^{st}$ network and other networks to the end are quadratic matrices of sizes $L\times L$ and shapes

$$\boldsymbol{A}_{k+1}=\begin{bmatrix}\boldsymbol{1} & \boldsymbol{0} & \boldsymbol{0}\\ \boldsymbol{0} & \boldsymbol{A}_{k+1}^{r} & \boldsymbol{0}\\ \boldsymbol{0} & \boldsymbol{0} & \boldsymbol{1}\end{bmatrix},\quad \boldsymbol{B}_{k+1}=\begin{bmatrix}\boldsymbol{0} & \boldsymbol{0} & \boldsymbol{0}\\ \boldsymbol{0} & \boldsymbol{B}_{k+1}^{r} & \boldsymbol{0}\\ \boldsymbol{0} & \boldsymbol{0} & \boldsymbol{0}\end{bmatrix}, \quad (25)$$

$$\boldsymbol{C}_{k+1}=\begin{bmatrix}\boldsymbol{0} & \boldsymbol{0} & \boldsymbol{0}\\ \boldsymbol{0} & \boldsymbol{C}_{k+1}^{r} & \boldsymbol{0}\\ \boldsymbol{0} & \boldsymbol{0} & \boldsymbol{0}\end{bmatrix} \quad \text{and} \quad \boldsymbol{D}_{k+1}=\boldsymbol{1}. \quad (26)$$

The matrices $\boldsymbol{A}_{k+1}^{r}$, $\boldsymbol{B}_{k+1}^{r}$ and $\boldsymbol{C}_{k+1}^{r}$ are matrices of the $k+1^{st}$ network with a real number of ports, and their sizes are $L_1\times L_1$, $L_1=n-m+1$.

The output voltage vector $\boldsymbol{U}_{2T,2}^{k}$ is the input voltage vector for the next $k+1^{st}$ network, and the output voltage vector for the $k+1^{st}$ open-ended network is

$$\boldsymbol{U}_{2T,2}^{k+1}=[\boldsymbol{A}_{k+1}^{r}+\boldsymbol{Z}_{22}^{k}\cdot\boldsymbol{C}_{k+1}^{r}]^{-1}\cdot\boldsymbol{U}_{2T,2}^{k}. \quad (27)$$

The *ETS* impedance matrix for the $k+1^{st}$ open-ended network is

$$\boldsymbol{Z}_{2T,2}^{k+1}=[\boldsymbol{A}_{k+1}^{r}+\boldsymbol{Z}_{22}^{k}\cdot\boldsymbol{C}_{k+1}^{r}]^{-1}\cdot[\boldsymbol{B}_{k+1}^{r}+\boldsymbol{Z}_{22}^{k}\cdot\boldsymbol{D}_{k+1}^{r}]. \quad (28)$$

The procedure for the solution of cascade-connected networks with a reduced number of ports is as follows:

1. The relations (5) and (6) are used to obtain $\boldsymbol{U}_{2T}^{k}$ and $\boldsymbol{Z}_{2T}^{k}$, i.e. *ETS* voltages and impedances for the first k cascade-connected networks with the same number of input and output ports. This vector and matrix are used for the input ports of the next $k+1^{st}$ cascade-connected network.
2. The matrices $\boldsymbol{A}_{k+1}^{r}$, $\boldsymbol{B}_{k+1}^{r}$ and $\boldsymbol{C}_{k+1}^{r}$ are formed for the $k+1^{st}$ network with $2L_1$ ports.
3. At the junction between k^{th} and $k+1^{st}$ networks, because of the reduced number of input ports, it is necessary to get only voltage vector $\boldsymbol{U}_{2T,2}^{k}$ from vector $\boldsymbol{U}_{2T}^{k}$ and matrix $\boldsymbol{Z}_{22}^{k}$ from matrix $\boldsymbol{Z}_{2T}^{k}$ (Eqs. (24) and (23)). The voltage vector $\boldsymbol{U}_{2T,2}^{k+1}$ and impedance matrix $\boldsymbol{Z}_{2T,2}^{k+1}$ are calculated from relations (27) and (28).
4. For further calculations, $k+2, k+3,..., K+3$, it is assumed that $\boldsymbol{Z}_{2T}^{k+1}=\boldsymbol{Z}_{2T,2}^{k+1}$, $\boldsymbol{U}_{2T}^{k+1}=\boldsymbol{U}_{2T,2}^{k+1}$, $\boldsymbol{A}\equiv\boldsymbol{A}^{r}$, $\boldsymbol{B}\equiv\boldsymbol{B}^{r}$, $\boldsymbol{C}\equiv\boldsymbol{C}^{r}$ and $\boldsymbol{D}\equiv\boldsymbol{D}^{r}=\boldsymbol{1}$ and the relations (5) and (6) can be used for solving the rest of the networks in the network cascade connection.

The suggested procedures are incorporated in the program *FAMIL* (*F*requency *A*nalysis of *MI*crowave *L*ines) [2] created in MATLAB [14].

IX. Analysis Results

A. ETS Method Efficiency Analysis

In order to reconsider the efficiency of the suggested *ETS* method, *2D* electrical circuits of various complexities are solved. The equivalent circuit composed as cascade-connected multi-port subnetworks shown in Fig.5 is analysed. The number of input ports is $L=10$ and the number of cascade-connected networks is $K=1,2,\cdots,200$. In this case, the largest equation system has 2000 unknown voltages. The efficiency testing program is done in MATLAB on PC 1.7 *GHz*.

Graphs of time needed for the solution of the equation system versus the number of network in cascade connection K, are depicted in Fig.10. The time needed for the forming of admittance matrix of *2D* circuit is included in the time needed for the solution of the equation system for all procedures. The MATLAB built-in functions are used for Gauss's procedure and matrix inversion procedure. The expressions given in this paper are used for the *ETS* method [2].

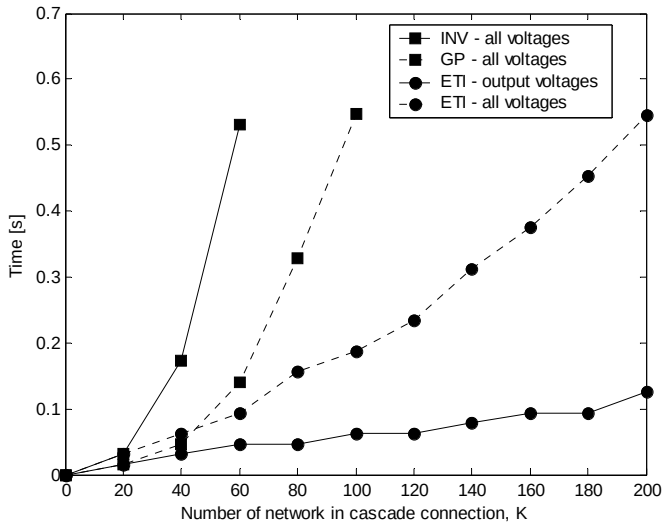

Fig.10. Efficiency curve graph.

From Fig.10 it can be inferred that the matrix inversion procedure requires the longest time needed for the solving of the equation system. In that case, a full admittance matrix is solved. The full admittance matrix is also solved by Gauss procedure, but it is more efficient than the matrix inversion procedure. The *ETS* method does not require the calculation of current vectors and, because of that, it is the most efficient method in the case when all voltages are to be calculated. The essential advantage of the *ETS* method is the calculation of output voltages only, which is the most common case in practice.

B. Microstrip Open-ended Line

Consider a rectangular microstrip line on a $100\,\mu m$ GaAs substrate with $\varepsilon_r = 12.9$ shown in Fig.11 [2]. The strip width is $w = 50\,\mu m$ and the length $d = 100\,\mu m$. A uniform microstrip line is an open-ended line with the source impedance of $R_S = 50\,\Omega$. The number of segments in the transversal direction is $L = 1$ and the number of segments in the longitudinal direction is $K = 1$.

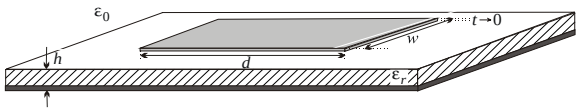

Fig.11. Geometry of a microstrip line.

Figs. 12 and 13 show a comparison between the results of the *MAPS* model, *HP Momentum*, a commercially available circuit simulator, [8], *ADS* and *FAMIL*. *MAPS* (Multidimensional Adaptive Parameter Sampling) [8] is an adaptive technique for building multidimensional parameterised analytical models for general planar microwave structures with a predefined accuracy and based on full-wave electromagnetic simulations. The results of *HP Momentum*, the *MAPS* model and *ADS* are virtually indistinguishable on the figure. The results of the circuit simulator differ significantly from those results and from our results obtained by the program *FAMIL*.

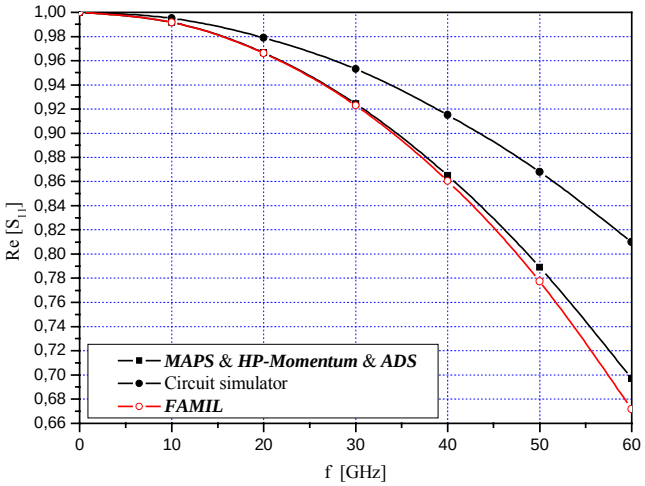

Fig.12. Real part of S_{11}.

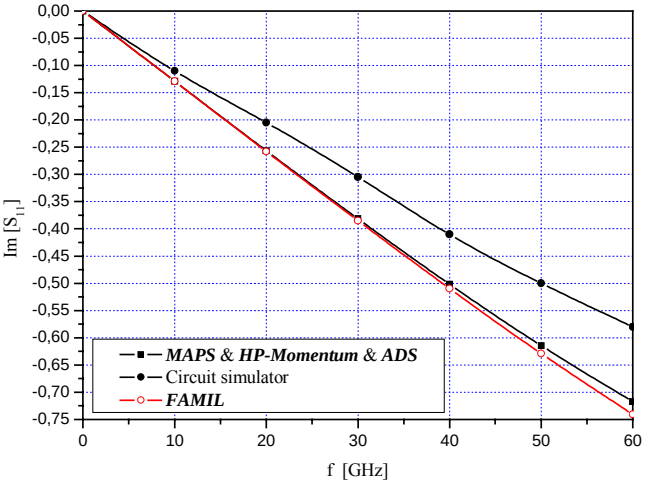

Fig.13. Imaginary part of S_{11}.

C. Microstrip Line Terminated in its Characteristic Impedance

Consider a rectangular microstrip line terminated in its characteristic impedance at both ends [2]. The segmentation in the transversal direction is not done, i.e. the number of network inputs is $L = 1$. Its length is equal to the wavelength on the line ($d = \lambda = 1700\,\mu m$ at $f = 60\,GHz$). The other geometrical and substrate parameters, except the number of network inputs and the number of cascade-connected ladder networks, are the same as those in the case of the microstrip open-ended line. The characteristic impedance of the line, without dispersion effects, is $Z_c = 58.26\,\Omega$.

A transmission line circuit with arbitrary source and load impedances, R_S and R_L, is shown in Fig.14. The transmission line is assumed to be lossless, with the length d and the characteristic impedance Z_c. This circuit is general enough to model most passive and active networks that occur in practice.

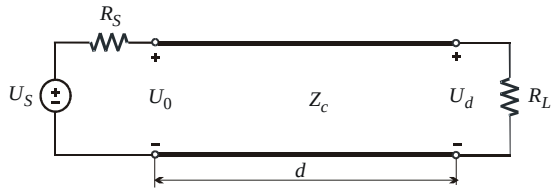

Fig.14. Lossless transmission line.

The output voltage is

$$U_d = \frac{1}{\left(1+\frac{R_S}{R_L}\right)\cos\theta + j\left(\frac{R_S}{Z_c}+\frac{Z_c}{R_L}\right)\sin\theta}\cdot U_S, \qquad (29)$$

where $\theta = \beta d = \omega d / v$ is the electric length of the transmission line and $v = c_0 / \sqrt{\varepsilon_r^{eff}}$ the phase velocity. The equation (29) gives an accurate result at each frequency.

TABLE 1
COMPARISON OF THE RESULTS

Freq. [*GHz*]	OUTPUT VOLTAGE MAGNITUDE			
	Transmission line solution Eq. (29)	*ETS method* $K=1$	*ETS method* $K=10$	*ETS method* $K=20$
0	0.5000	0.5000	0.5000	0.5000
10	0.5000	0.4957	0.5000	0.5000
20	0.5000	0.3432	0.5000	0.5000
30	0.5000	0.1346	0.5000	0.5000
40	0.5000	0.0586	0.4999	0.5000
50	0.5000	0.0301	0.4998	0.5000
60	0.5000	0.0175	0.5000	0.5000

Table 1 shows that the corresponding number of segments in the longitudinal direction, K, will give a better approximation in the wider frequency band. The results are given for the case when $L=1$ and $U_S=1$.

The magnitude of the scattering parameter S_{11} versus frequency, obtained by *FAMIL* and *ADS*, is shown in Figs. 15 and 16, respectively. The results obtained by the program *FAMIL*, i.e. *ETS* method, are in good agreement with those obtained by the program *ADS* [11].

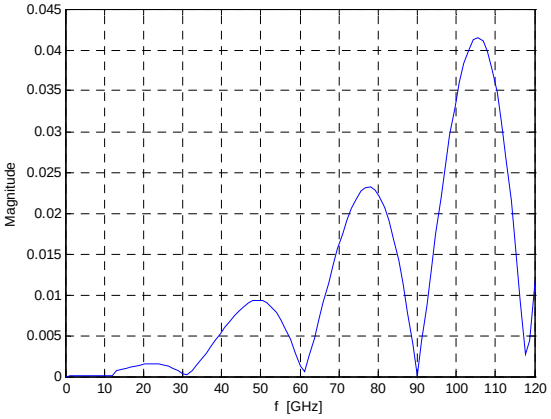

Fig.15. Magnitude of the scattering parameter S_{11} versus frequency for $K=40$ in the program *FAMIL*.

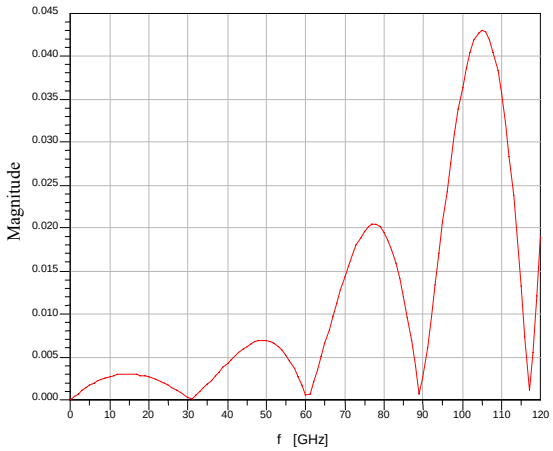

Fig.16. Magnitude of the scattering parameter S_{11} versus frequency in the program *ADS*.

D. Microstrip T - junction

Consider a microstrip *T*-junction depicted in Fig.17 [2]. The substrate material is Polyguide with the relative dielectric constant of $\varepsilon_r = 2.32$ and the board thickness $h = 1.58\,mm$.

In the program *FAMIL*, the *T*-junction is analysed as a cascade connection of five uniform transmission lines. Line widths are $w_1 = w_5 = 4.71\,mm$, $w_2 = w_4 = 20\,mm$ and $w_3 = 50\,mm$. Their lengths are $d_1 = d_5 = 30\,mm$, $d_2 = d_4 = 2.65\,mm$ and $d_3 = 4.71\,mm$. The filter is terminated in $50\,\Omega$ at both ends.

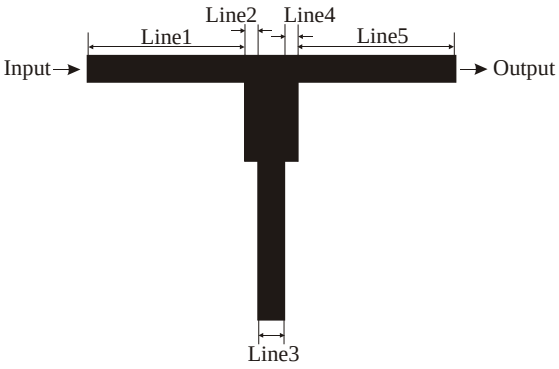

Fig.17. *T*-junction layout.

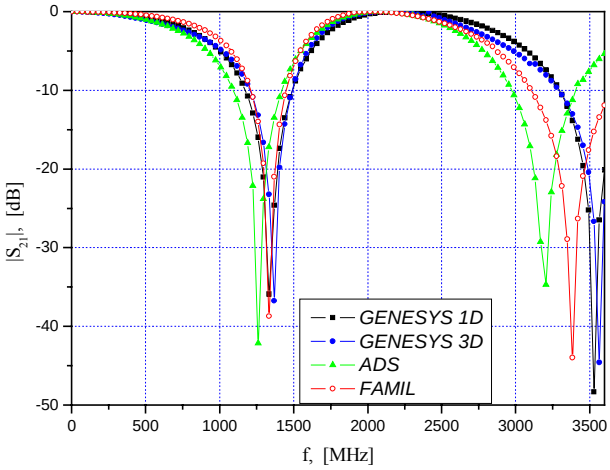

Fig.18. Magnitude of the transmission coefficient versus frequency.

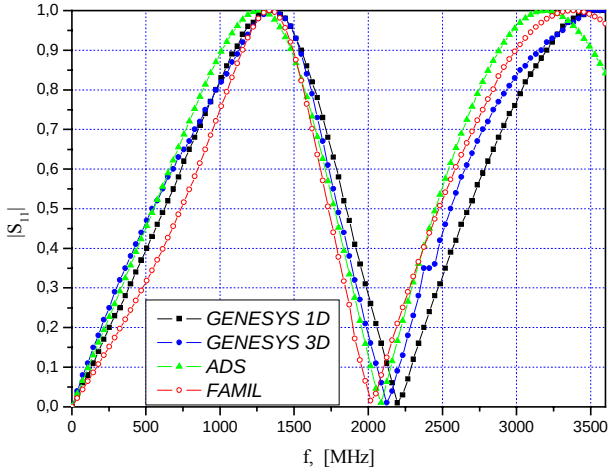

Fig.19. Magnitude of the reflection coefficient versus frequency.

The magnitude of the transmission and reflection coefficients versus frequency, obtained by the programs *GENESYS* (*1D* analysis using transmission lines and *3D* electromagnetic analysis) [12], *FAMIL* and *ADS*, are shown in Figs. 18 and 19.

From the responses given in Fig.18 it can be inferred that the response obtained by *FAMIL* is in better agreement with the one of electromagnetic simulation done in *GENESYS* than the response obtained by *ADS*.

E. Lowpass Filter I

Consider a lowpass filter with a layout shown in Fig.20. This filter is analysed in references [15]. The length of the first and third line is equal, $d_1 = d_3 = 15\,mm$.

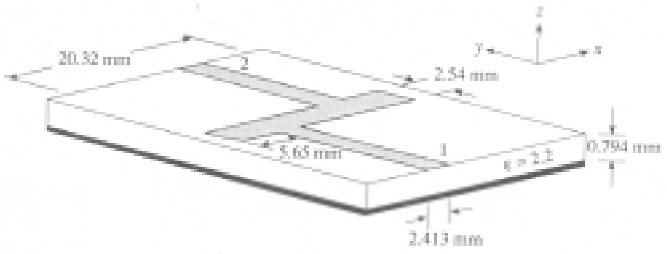

Fig.20. Layout of lowpass filter.

The number of segments in transversal and longitudinal directions has a great significance when this filter or some other structures are analysed in the program *FAMIL*. The filter shown in Fig.19 is analysed as a cascade connection of three rectangular microstrip lines. The chosen line segmentations are $L = 1$ and $K = 20$ for the first and third lines and $L = 8$ and $K = 10$ for the second line.

Fig.21 shows the analysis results given in reference [15]. Here, measured results (MEASUREMENT), as well as results obtained by *3D FDTD* (*Finite-Difference Time-Domain*) method (CALCULATION), are given. The analysis results obtained in the program *FAMIL* are shown in Fig.22. The comparison of results given in Figs. 21 and 22 shows good agreement.

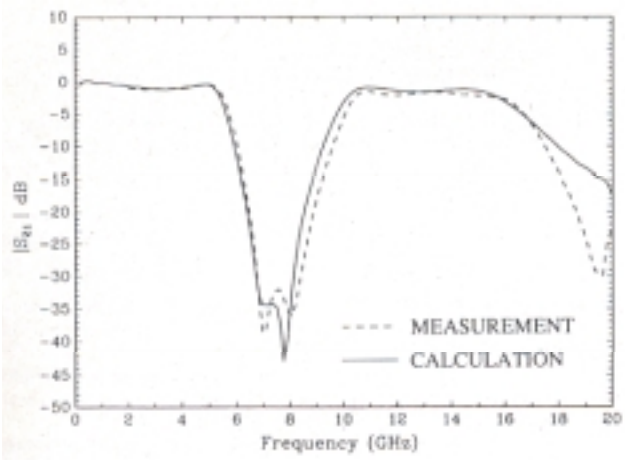

Fig.21. Results given in reference [15].

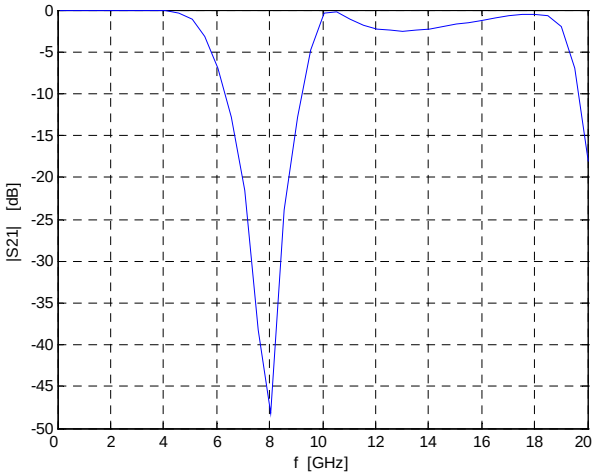

Fig.22. Lowpass filter frequency response obtained

by the program *FAMIL*.

F. Lowpass Filter II

Consider a microstrip stepped-impedance 7^{th} order Chebyshev lowpass filter with a cutoff frequency of $900\,MHz$ and $50\,\Omega$ terminations given in chapter 7.2 in reference [16]. The layout is shown in Fig.23. The nominal substrate dielectric constant is $\varepsilon_r = 6.0$, the board thickness is $h = 635\,\mu m$ and the strip thickness is $t = 18.03\,\mu m$.

Fig.23. Layout of stepped-impedance lowpass.

The stepped-impedance lowpass is a cascade of alternating high and low impedance transmission lines. The high impedance lines act as serial inductors and the low impedance lines act as shunt capacitors. The high impedance narrow lines are $465.19\,\mu m$ wide (line2, line4, line6 and line8) and the low impedance wide lines are $4811.52\,\mu m$ wide (line3, line5 and line7). The intermediate width lines at the ends ($w1 = w9 = 932.59\,\mu m$) are the $50\,\Omega$ leader lines. If the filter is terminated in $50\,\Omega$, the lengths of these leaders affect only filter dissipation loss and phase length.

This microstrip lowpass filter is observed as cascade-connected transmission lines with various lengths and increased or reduced widths. Their lengths are $d1 = d9 = 2540\,\mu m$, $d2 = d8 = 18114.91\,\mu m$, $d3 = d7 = 7834.46\,\mu m$, $d4 = d6 = 32042.02\,\mu m$ and $d5 = 9771.33\,\mu m$.

The results obtained by the program *FAMIL* are compared with the ones obtained by the program *GENESYS* and shown in Fig.24. The attenuation characteristics are in good agreement at lower frequencies. For higher frequencies the results differ slightly.

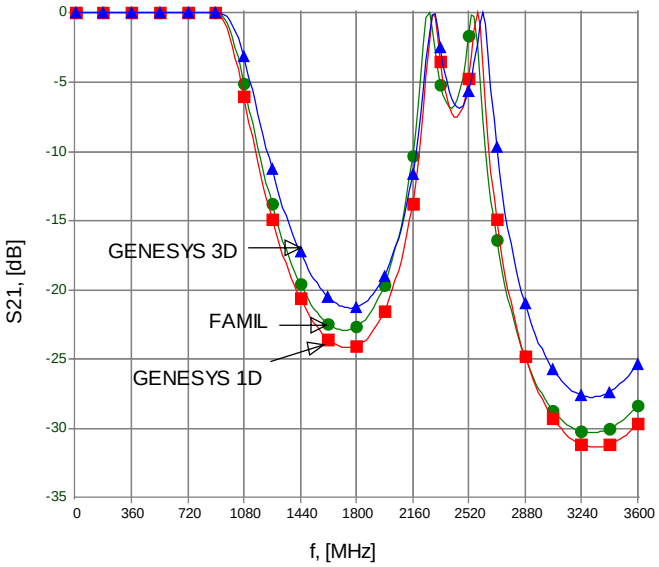

Fig.24. Frequency response of a microstrip lowpass filter.

G. Lowpass Filter III

Consider a microstrip lowpass filter with a cutoff frequency of $900\,MHz$ and $50\,\Omega$ terminations given in chapter 7.5 in reference [16]. The layout of the filter under consideration is shown in Fig.25. The nominal substrate dielectric constant is $\varepsilon_r = 6.0$, the board thickness is $h = 635\,\mu m$ and the strip thickness is $t = 18.03\,\mu m$.

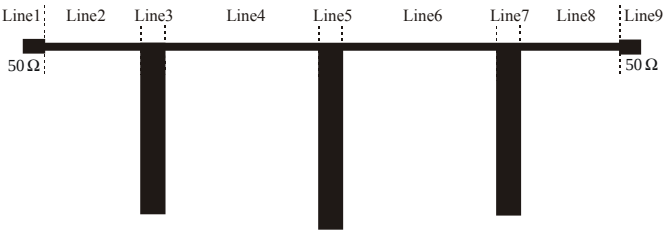

Fig.25. Layout of lowpass filter.

The lines at the ends (line1 and line9) are $50\,\Omega$ leader lines. If the filter is terminated in $50\,\Omega$, the lengths of these leaders affect only filter dissipation loss and phase length.

The microstrip lowpass filter is observed as nine cascade-connected transmission lines with various lengths and increased or reduced widths. The widths of transmission lines are $w1 = w9 = 932.59\,\mu m$, $w2 = w4 = w6 = w8 = 465.19\,\mu m$, $w3 = 15679.79\,\mu m$, $w5 = 18016.59\,\mu m$, $w7 = 15781.39\,\mu m$. Their lengths are $d1 = d9 = 2540\,\mu m$, $d2 = 13385.80\,\mu m$, $d3 = d5 = d7 = 2873.93\,\mu m$, $d4 = d6 = 30022.80\,\mu m$ and $d8 = 13436.60\,\mu m$.

The result obtained by the program *FAMIL* and the ones obtained by electromagnetic and linear simulations in the program *GENESYS* are depicted in Fig.26. From the responses it can be inferred that the response obtained by *FAMIL* is in good agreement with that of electromagnetic simulation done in *GENESYS*.

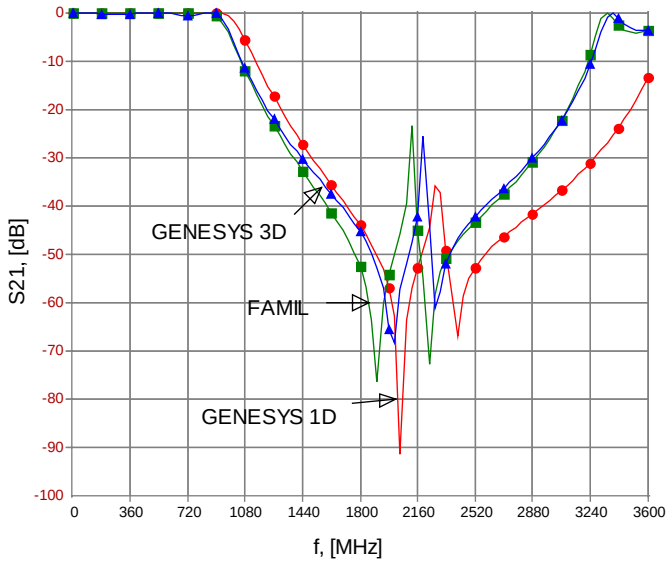

Fig.26. Response of a microstrip lowpass filter.

X. CONCLUSION

Each phase of procedure for frequency analysis of microwave lines based on the Equivalent Thevenin Source (*ETS*) method is described in references [1-6]. The microwave structure is treated as a cascade connection of uniform transmission lines with various lengths and equal, increased or reduced widths. In this paper, the complete analysis procedure with corresponding relations is given.

The purpose of this paper is to show that the frequency analysis of planar transmission lines based on the *ETS* method can be a strong competitor to other known methods. It leads to a universal and effective computer program capable of solving a wide range of practical problems called *FAMIL* (***F***requency ***A***nalysis of ***MI***crowave ***L***ines) [2].

The efficiency and accuracy of the suggested procedure is shown in a few various examples realized in the microstrip line technique, such as open-ended line, line terminated in its characteristic impedance, *T*-junction and lowpass filters. The results of the analysis obtained by the program *FAMIL* have shown good agreement with those obtained by other programs mentioned above.

The analysis procedure described here can be applied to both symmetrical and asymmetrical connections of transmission lines with different lengths and widths. This procedure may be further generalized to analyze any type of various tapered microstrip transmission lines.

ACKNOWLEDGEMENT

This work has been supported by the Ministry of Science and Enviroment Protection of the Republic of Serbia.

REFERENCES

[1] B. Stojanovi} and M. Gmitrovi}, “Planar Transmission Line Analysis”, *XVLI Yugoslav Conference - ETRAN*, June 3-6, 2002, Banja Vru}ica - Tesli}, Republic of Srpska, pp. 241-244.

[2] B. Sto{i}, *Frequency Analysis of Planar Microwave Circuits by Thevenin Source Method,* Master thesis, Faculty of Electronic Engineering, University of Ni{, Ni{, February 2004, (in Serbian).

[3] B. Stojanovi} and M. Gmitrovi}, “Analysis of 2D Lumped Circuit by Equivalent Thevenin Source Method”, *14th International Conference on Microwaves, Radar and Wireless Communications - MIKON 2002*, May 20-22, Gdansk, Poland, pp. 549-552.

[4] B. Stojanovi} and M. Gmitrovi}, “Analysis of Cascade-Connected Transmission Lines with Different Widths by ETS Method”, *X Telecommunication Forum - TELFOR 2002*, November 26-28, Belgrade, Yugoslavia, pp. 595-598.

[5] M. Gmitrovi} and B. Stojanovi}, “Analysis of Cascade-Connected Planar Transmission Lines by ETS Method”, *XXXVII International Scientific Conference on Information, Communication and Energy Systems and Technologies - ICEST 2002*, October 1-4, Ni{, Yugoslavia, Volume 1, pp. 317-320.

[6] B. Stojanovi} and M. Gmitrovi}, “Modeling and Analysis of Cascade-Connected Planar Transmission Lines”, *XII International Symposium on Theoretical Electrical Engineering - ISTET’03*, Poland, Warsaw, July 6-9, 2003, Volume II, pp. 473-476.

[7] J.H. Thompson, T.R. Apel, “Simplified Microstrip Discontinuity Modeling Using the Transmission Line Matrix Method Interfaced to Microwave CAD”, *Microwave Journal*, July 1990, pp. 79-88.

[8] J. D. Geest, T. Dhaene, N. Fache and D. De Zutter, “Adaptive CAD-Model Building Algorithm for General Planar Microwave Structures”, *IEEE Transactions on Microwave Theory and Techniques*, Vol. 47, No. 9, September 1999, pp. 1801-1808.

[9] W. K. Gwarek, “Analysis of Arbitrarily Shaped Two-Dimensional Microwave Circuits by Finite-Difference Time-Domain Method”, *IEEE Transactions on Microwave Theory and Techniques*, Vol. 36, No. 4, April 1998, pp. 738-744.

[10] Touchstone and Libra User’s Manual, HP 851701A, Touchstone Family Software, January 1990.

[11] Advanced Design System 2002, Agilent Technologies 1983-2002, 395 Page Mill Road, Palo Alto, CA 94304, USA.

[12] RF and Microwave Design Software GENESYS, Eagleware Corporation, 635 Pinnacle Court, Norcross, GA 30071, 2001.

[13] I. Bahl and P. Bhartia, *Microwave Solid State Circuit Design*, John & Wiley Sons, Inc., USA, 1988.

[14] MATLAB – The Language of Technical Computing, Version 6.5.0.180913a, Release 13, June 18, 2002, The Math Works Inc. 1984-2002.

[15] D. M. Sheen, S. M. Ali, M. D. Abouzahra and J. Au Kong, “Application of the Three-Dimensional Finite-Difference Time-Domain Method to the Analysis of Planar Microstrip Circuits,” *IEEE Transactions on Microwave Theory and Techniques*, Vol. 38, No. 7, July 1990, pp. 849-857.

[16] R. W. Rhea, *HF Filter Design and Computer Simulation*, Noble Publishing Corporation, USA, 1994.